
Article:
Lu, Keding, Wang, Hongli, Liu, Yanhui et al. (8 more authors) (2022) Unexpected Fast Radical Production Emerges in Cool Seasons:Implications for Ozone Pollution Control. National Science Open. 20220013. ISSN: 2097-1168

https://doi.org/10.1051/nso/2022007

RESEARCH ARTICLE

National Science Open
1: 20220013, 2022
https://doi.org/10.1360/nso/20220013

Earth and Environmental Sciences

Special Topic: Emerging Pollution and Emerging Pollutants

Unexpected fast radical production emerges in cool seasons: implications for ozone pollution control

Hongli Wang[1,#], Yanhui Liu[2,#], Xiaorui Chen[2,#], Yaqin Gao[1], Wanyi Qiu[2], Shengao Jing[1], Qian Wang[1], Shengrong Lou[1], Peter M. Edwards[3], Cheng Huang[1,*] & Keding Lu[2,*]

[1]*State Environmental Protection Key Laboratory of Formation and Prevention of Urban Air Pollution Complex, Shanghai Academy of Environmental Sciences, Shanghai 200233, China;*

[2]*State Key Joint Laboratory of Environmental Simulation and Pollution Control, College of Environmental Sciences and Engineering, Peking University, Beijing 100871, China;*

[3]*Wolfson Atmospheric Chemistry Laboratories, Department of Chemistry, University of York, York YO1 7EP, UK*

#Contributed equally to this work.

*Corresponding authors (emails: k.lu@pku.edu.cn (Keding Lu); huangc@saes.sh.cn (Cheng Huang))

Received 21 August 2021; Revised 12 October 2021; Accepted 17 January 2022; Published online 26 April 2022

Abstract: Ozone is a crucial air pollutant that damages human health and vegetation. As it is related to the photo-oxidation of the nitrogen oxides and volatile organic compounds, the summertime reduction of these precursors is the primary focus of current ozone mitigation strategies. During ozone pollution episodes in eastern China, an observed accumulation of daily total oxidants (O_x=NO_2+O_3) in cool seasons (spring and autumn: 60 ppb and winter 40 ppb) is comparable to that in summer (60 ppb), indicating fast photochemical production of secondary pollutants including ozone over the year. Unrecognized fast radical primary productions are found to counteract the increased termination of hydroxyl radical and unfavorable meteorological conditions to maintain the rapid total oxidant formations in cool seasons. Elucidating and regulating the primary radical sources may be critical for the secondary air pollution control in cool seasons.

Keywords: OH radical, photochemistry, VOCs, ozone, air pollution

INTRODUCTION

Tropospheric ozone (O_3) is formed primarily via the photolysis of nitrogen dioxide (NO_2), which is a product of reactions between nitrogen monoxide (NO) and various oxidants including hydroxyl peroxy radical (HO_2), organic peroxy radicals (RO_2), and O_3 itself [1]. The peroxy radicals (HO_2 and RO_2) are primarily produced from the oxidation of VOCs by the hydroxyl radical (OH) and the concentrations of OH radical were shown to be correlated well with the solar radiations in the troposphere [2]. Thus, strong solar radiation and sufficient precursors (NO_x and VOCs) are the prerequisites to enable fast O_3 productions. It was generally recognized and observed that, in the northern mid-latitude urban areas, photochemical O_3 production peaks in summer and becomes considerably lower in cool seasons (i.e., spring, autumn, and winter).

Fast photochemistry in winter resulting in substantial O_3 formation has been previously reported. In the

basins of the US, high O_3 concentrations up to 140 ppb were observed in winter during the stagnant meteorological conditions with abundant VOCs emissions from gas and oil productions [3,4]. Since O_3 can be titrated by NO to produce NO_2 in high NO_x environments, the sum of O_3 and NO_2 is frequently used as an indicator of the total oxidant namely O_x. Up to 150 ppb of O_x was observed in winter in Beijing [5] and up to 80 ppb in winter in Salt Lake Valley [6] during heavy haze episodes, respectively. An up to 93% increase of the afternoon O_3 concentration was found in the winter time (December, January, February) in Guanzhong basin from 2013 to 2019, indicating a higher oxidation capacity and a more rapid photochemistry [7]. Recent studies also reported that O_3 pollution events occurred in China in January–February 2020 due to the low NO_x emissions during the lockdown period of COVID-19 [8]. These new findings set up questions that why fast photochemistry can happen under low solar radiation conditions and even with higher frequency.

Studies were carried out to understand the winter time radical behaviour. During winter in the Utah Basin, fast radical production was diagnosed to be dominated by the photolysis of the oxygenated VOCs which is generated from the VOCs released during natural gas production nearby and trapped in a very shallow boundary layer. Also, thick snow cover compensates the low solar zenith angles with high albedo in winter, resulting in fast O_3 formation [3]. This is not the case for most of the cities. Underestimation of HO_x, especially HO_2 by the Observational Based Model under a high NO_x environment in winter, has been reported in various other locations, such as New York City [9], Tokyo [10] and Beijing [11,12], which indicated radical production sources are missing. HONO photolysis has been found to be one of the major sources of HO_x in the day during winter [10,13], followed by ozonolysis of alkenes. The high wintertime OH concentrations in the urban UK was found to be driven by ozonolysis of alkenes [14,15].

This study analyzed O_3 measurement data from 2013 to 2019 and showed that in Eastern China surface O_3 concentrations in all major city clusters increased in the recent decade and the non-attainment cases started to appear not only in summer but in cool seasons (as early as March and as late as November) (Supplementary Figures S1 and S2). Based on continuous measurements, this study quantitatively investigates wintertime O_x formation mechanisms and radical production by conducting the emission driven box model simulations. More details about the measurements and the model are included in the Methods and Supplementary Information. The contribution of radical precursors has been studied with the sensitivity test runs. Based on the conclusions, we also proposed a new O_3 mitigation concept which included the consideration of radical initiation processes in addition to the conventional control on NO_x and VOCs.

SEASONAL OZONE POLLUTION CHARACTERISTICS IN SHANGHAI

The monthly variation of maximum daily averaged 8 h (MDA8) O_3 non-attainment rate in Shanghai shows that O_3 pollution episodes occurred in cool seasons with increasing frequency from 2013 (0.5%) to 2019 (6.9%), which might be a result from stronger photochemistry with reduced haze responding to the NO_x and SO_2 emissions control since 2013 (Figures 1A and S3). In 2018 and 2019, the highest MDA8 O_3 non-attainment rate occurred in spring (May) rather than summer (June, July and August) when monthly temperature and the solar radiation reached their peaks (Figure S4). High O_3 events were even recorded in March, October and November, which indicates an efficient O_3 production in the cool weather. The three-year (2017 to 2019) measurements show that the total summed OH reactivity (the aggregate reaction frequencies with

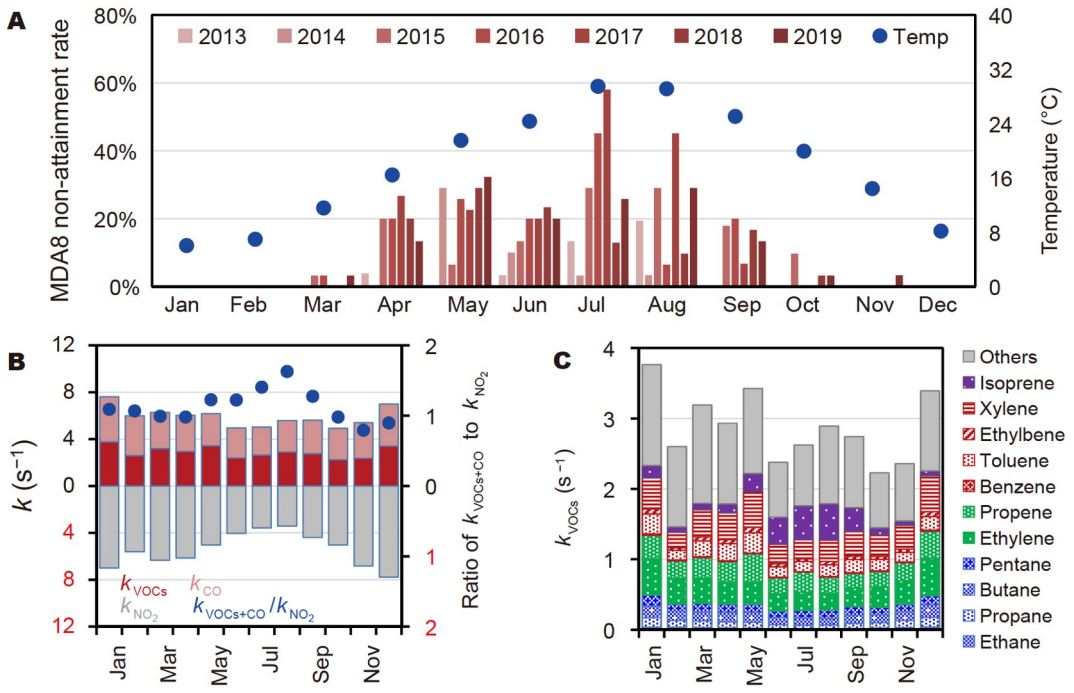

Figure 1 Monthly characteristics of ozone pollution and its precursors in the Shanghai metropolitan area. (A) Monthly pattern of MDA8 over the National Air Quality Standard (160 μg/m^3) rates from 2013 to 2019, and the monthly temperature from 2013 to 2019. (B) Monthly pattern of the OH reactivity of the observed VOCs (k_{VOCs}), CO (k_{CO}), and NO_2 (k_{NO_2}), and the ratio of (k_{VOCs} + k_{CO}) to k_{NO_2}, which were the average results from January 2017 to December 2019. (C) Monthly pattern of the composition of k_{VOCs}.

OH for all chemicals calculating as the reaction rate constant times the ambient concentrations of various chemicals, which is also the inverse of the OH lifetime) from carbon monoxide (CO), NO_2, and the VOCs are relatively similar for different seasons (Figure 1B). The observed total summed OH reactivity is slightly higher in winter and lower in summer, which is mainly driven by the high NO_2 and CO in winter. The change of the total VOCs is less profound for different seasons, and it is likely that the enhanced contribution of biogenic emissions and evaporation of solvent/oil gases is balanced out by the concurrent stronger dilution effect under the higher temperatures [16] (Figures 1C and S5). The ratio of the OH reactivity related to VOCs plus CO to that of NO_2 can reach approximately 1.5 in summer when lowest NO_2 appears, while it is quite stable around 1.0 in other seasons indicating the deficiency of VOC sources. Our simulations of the box model also suggest that Shanghai is under VOCs-limited regime for the O_3 production. It is then interesting to see that why O_3 pollutions can still take place with elevated NO_x concentrations during the cool seasons even in a VOCs-limited regime. A possible reason is that NO_x and VOCs concentrations are high in winter due to a shallower boundary layer and weaker dilution, in which case O_3 concentration is also condensed leading to a pollution episode.

DEPENDENCES OF THE OBSERVED DAILY OZONE ACCUMULATIONS VERSUS TEMPERATURE

The total oxidant ($O_x = O_3 + NO_2$) has been used as an indicator to quantify the photochemical production of

O_3 despite the interconversion between O_3 and NO_2 [17,18]. Compared with O_3, it is also a less variable parameter from spacial and temporal perspectives (Figures S6–S8). The diurnal variations of O_x in different seasons show similar trend (Figures 2A, 2D and 2G) based on the past three-year measurements. O_x peaks in the early afternoon (13:00–14:00) and reaches its minimum in the early morning (6:00–7:00). The difference between the two is defined as daily accumulations of O_x, which is referred to as ΔO_x in the following text. ΔO_3 is calculated in the same way (Figure S9). In this study, the cool season bins are the bins with mean temperature lower than 18°C since the composition of summer data is lower than 10% (Figure S10). Interestingly, O_x concentration in cool seasons is at the similar level as that in warm seasons (black line), whereas the mid-summer O_x level (blue line) is slightly lower (Figures 2A, 2D, and 2G). No dependence of daily averaged O_x (black) on temperature was observed in Shanghai, Yangtze River Delta (YRD) and North China Plain (NCP), though solar radiation intensity and condition of precursors vary significantly in different seasons. This is not true for the daily averaged O_3. Figure S9 shows that higher O_3 concentrations tend to appear under higher temperatures. It means that the atmospheric oxidations in cool season was as strong as that in warm season from the total oxidant perspective, and O_3 was just more in the form of NO_2 through reaction with NO. High levels of ΔO_x were observed at the low temperatures (i.e., <18°C) in all three regions, although still slightly lower compared with those at high temperatures (18°C–25°C), which is like to be a result of higher background O_x for the cool seasons (Figures 2A, 2D and 2G) [19]. High O_3 production in cool seasons suggests that O_3 control is not only a summer issue in Eastern China. Both ΔO_x and ΔO_3 (red) showed a broad curved and weak dependence on the changes of the ambient temperature. Bigger differences between ΔO_x and daily O_x concentration were observed in cool seasons than they were in summer, which indicates the high background O_x concentration can be partly due to a longer lifetime of O_x in low temperature and low radiation. Hence, accumulation of the O_x produced in cool seasons can be more effective due to the longer lives.

The concentrations of VOCs and NO_2 were highly correlated over the change of the temperatures (Figure 2C), and VOCs and NO_2 are highly correlated as well (Figure S11). From a phenomelogical perspective, the reduced solar radiation was compensated by the increased concentrations of NO_x and VOCs resulting in a regime where O_3 is formed efficiently.

EXPLORATION OF THE DRIVEN FORCE FOR PHOTOCHEMISTRY IN COOL SEASONS

To explore reasons of this fast photochemistry in the cool seasons, emission driven box model simulations were conducted (Methods and Supplementary Information) for temperature bins below 25°C and illustrated in Figure 3A (red solid line). Wind speed is significantly higher in the bins of mid-summer (>25°C, Figure S12), indicating a strong dilution effect which makes the air not stagnant enough for the box model simulation. Also, this study mainly focused on the fast oxidation during cool seasons rather than summer. Hence three bins under high temperature condition were excluded. The box model simulations were adjusted and optimized according to comprehensive measurements of CO, NO_x and VOCs (Table S1) from an urban supersite in Shanghai. Further details on model performance are in Methods. In the warm seasons (18°C–25°C), the model simulated ΔO_x showed good agreement with the observational data, whereas considerable underestimations are simulated in the cool season when the temperature is below 18°C (Figure 3A). Given

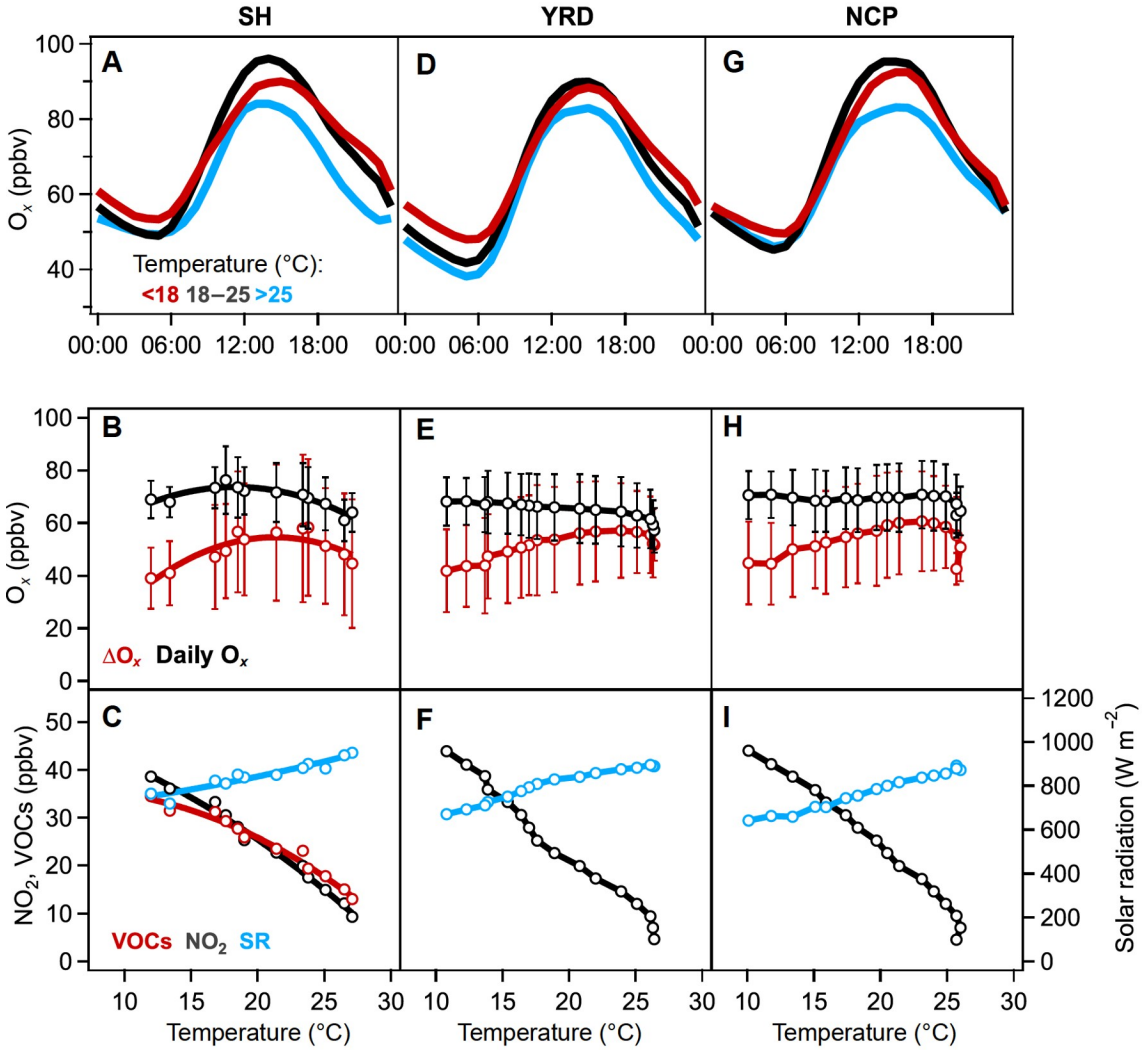

Figure 2 Observed diel variation of O_x (=O_3+NO_2), and relationship of the ΔO_x as well as daily averaged data for O_x, NO_2, VOCs and solar radiation with temperature during high O_x (maximum hourly averaged O_x >75 ppbv) days in Shanghai, YRD, and NCP regions. The sunny day (maximum of solar radiation>550 W m^{-2}) observations were analyzed based on measurements from 2017 to 2019 of the national monitoring network. Results of Shanghai include 9 sites, that of YRD region include 180 sites in 41 major cities and that of NCP include 140 national monitoring sites in 30 major cities (Figure S1B). Values are averages over 2.5 ppbv NO_2 bins for the daily average (at least 10/50 data points required in city/regional scale). The daily average data of VOCs during the same period were from an urban supersite in Shanghai. The meteorological variables were from the Surface Meteorological Stations in China. (A), (D), (G) Diel variation of O_x during photochemical smog days in Shanghai, YRD and NCP, respectively. The red, black and blue lines represent three temperature bins: <18°C, 18°C–25°C and >25°C, which indicate cool seasons, warm seasons and mid-summer. (B), (E), (H) Dependences of the daily averaged O_x and daily ΔO_x on averaged temperature. (C), (F), (I) Relationships of daily averaged NO_2, VOCs and maximum solar radiation (SR) with the average temperature in Shanghai, YRD and NCP, respectively. The error bars indicate the standard variations.

that the air mass was stagnant in the cool seasons according to the low wind speed (Figure S12), we made sensitivity test on reducing the physical loss (dilution rate) up to a factor of two, which only showed marginal enhancement on the simulated ΔO_x. Thus, the up to 50% underestimation of ΔO_x during lower temperature is considered to be related to the chemical processes. As the photolysis rates are constrained to observations and the concentrations of alkenes are validated with the measurements, the chemical sinks of O_x shall be represented reasonably well, indicating a strong missing chemical production of O_x in the model during the

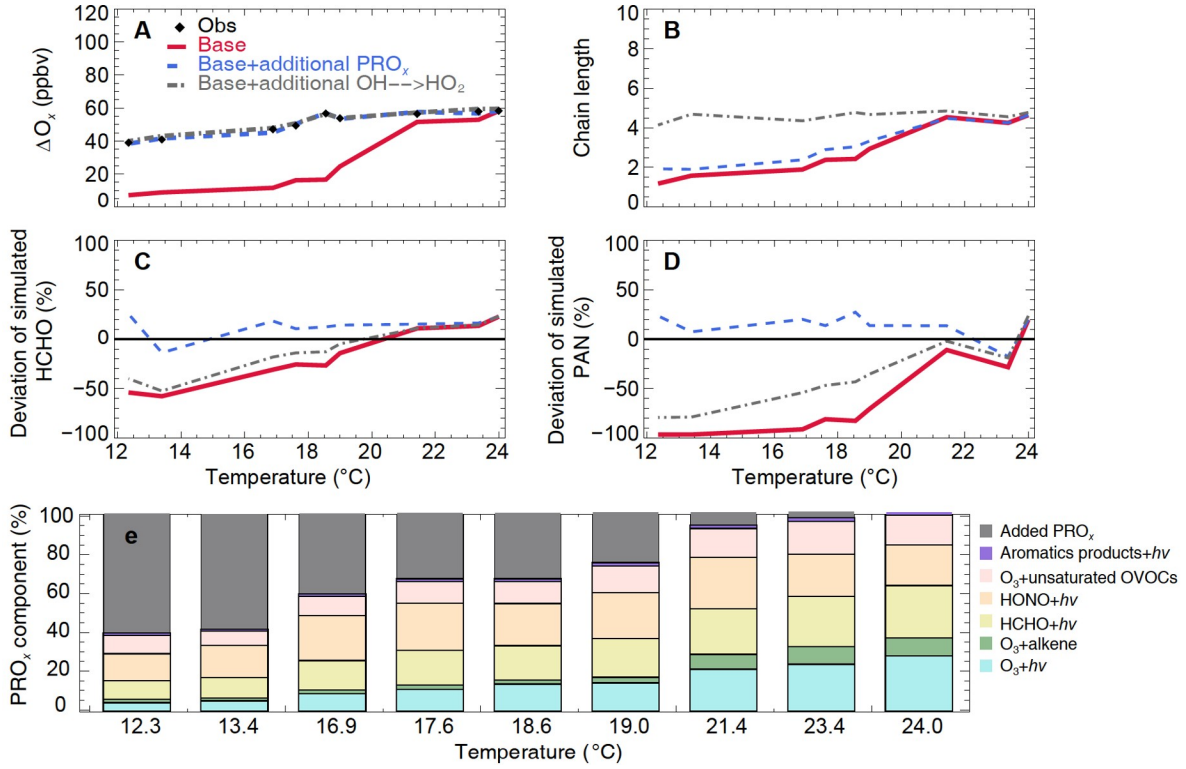

Figure 3 Observed and modelled dependence of the photochemical indicators on the change of temperature. (A) Daily accumulated O_x productions. (B) ChL of OH propagation. (C), (D) Deviation of the simulated concentrations of HCHO and PAN to the observations, respectively. The compositions of simulated primary RO_x production (PRO_x) in the selected bins are shown in (E). Details of the model runs are referred to in the main text and Methods.

cool seasons.

Theoretically, the instantaneous photochemical O_3 production rates can be considered as the product of the primary RO_x (= OH + HO_2 + RO_2) radical production (PRO_x) and an amplification factor—chain length (ChL) of the cycling. The ChL is an indicator of the efficiency of OH-HO_2-RO_2 cycle, and it is dependent on the ambient environment such as the concentrations of NO_x and VOCs [20]. In the traditional O_3-NO_x-VOCs sensitivity analysis framework, the cycle of the OH-HO_2-RO_2 is often analyzed under fixed PRO_x [21–23]. However, PRO_x can change several times depending on the ambient air compositions and meteorology conditions [11,24].

Good agreement of ΔO_x can be achieved when up to 3.5 ppb/h additional PRO_x, and extra PRO_x in the form of additional OH production scaled with the change of solar radiation (Figure S13) are added (blue dashed line in Figure 3A). Previous studies found that HO_x, as well as RO_2 is underestimated by 2 to 5 times during high NO_x conditions in winter of Beijing and a maximum of 5 ppbv/h of missing PRO_x is calculated, which is consistent with our results [11,12]. The photochemical oxidation processes seem to be better described with this change in cool seasons as notable improvements are seen in HCHO and PAN simulations (Figures 3C and 3D). The compositions of PRO_x in each bin are illustrated in Figure 3E. The most striking feature is a negative correlation between the additional PRO_x needed to maintain the observed ΔO_x and temperature. Based on the model simulation, ozone photolysis becomes less important to the RO_x production with the decreasing temperature, while the photolysis of HONO and HCHO is the major known sources of RO_x over

the year (Figure 3E). The potential candidates that can contribute to the underestimated PRO_x include radical precursors from direct emissions (e.g., OVOCs) and heterogeneous productions (e.g., $ClNO_2$) [3,5,15].

We also extended the sensitivity tests by various scenarios that might explain the missing O_3 production, such as increase of the ChL. In the test run, extra CO was added to the model to counteract the termination reactions, which amplifies the ChL by enhancing the conversion of OH to HO_2 without other associated effects on our results (Figure 3B). The observed ΔO_x can be reproduced if the ChL of the OH, HO_2 and RO_2 cycle is about twice in the base run (Figure 3E). The observed ΔO_x can be replicated if the ChL of the OH, HO_2 and RO_2 cycle is twice as much as it is in the base run (Figures 3A, 3B and S14). Nevertheless, the observed concentrations of HCHO and PAN are greatly underestimated in this model run, indicating that the model does not represent the chemical processes in the real world. Hence, the observed high ΔO_x cannot be simply explained by increasing ChL. Previous study found that a missing pathway that converts RO_2 to HO_2 and HO_2 to OH is lacking in the model, which is referred to as unclassical OH regeneration mechanism [25]. We also tested this mechanism to enhance ChL by adding X species to react with RO_2 and HO_2 producing HO_2 and OH, respectively. The maxima concentration of X is 0.8 ppbv equivalent of NO_x in the model (Figure S15). Therefore, we can conclude that the main reason for the underestimated ΔO_x for the cool seasons diagnosed in this study shall be attributed to the underestimated PRO_x. As the missing PRO_x was found for the high NO_x regime in several previous studies carried out in different locations and seasons [5,11,12,26], the diagnosis in this study also fit well with the previous findings.

POLICY IMPLICATIONS

Unexpected fast production of O_3 leading to pollution events were found in cool seasons in the whole Eastern China by analyzing the daily accumulative total oxidant, ΔO_x. O_x, including O_3 and NO_2, a key indicator of the oxidation capacity, which is crucial for not only O_3 production but also the formation of secondary aerosols [27,28]. In summer when NO_x is relatively low, ΔO_x mostly represents the chemical accumulation of O_3. However, during cool seasons considerable amount of O_3 is titrated by NO forming NO_2 leading to production of particulate nitrates and organic nitrates. With the remarkable improvement of particulate matters (PMs) pollutions but with increased partition of the secondary aerosols in China in recent years, the impact of O_3 pollution itself and the resulting high secondary particulate matter due to the high O_3 production rates [5,6] has become increasingly prominent.

Previous mitigation strategies in Eastern China mostly focused on O_3 during summer and $PM_{2.5}$ during winter. As a result, the current mitigation strategy focused on the control VOCs for summer O_3 and NO_x for winter PMs. As discussed earlier in this paper, though O_3 concentrations are relatively low in cool seasons, O_x concentrations remain high over the year (Figures 2B, 2E and 2H) and O_x is crucial to the formation of secondary pollutants including PMs.

The impact of the primary RO_x production on the daily accumulation O_x is discussed in detail above. As suggested in Figure 4A, the O_3 control objectives should include both RO_x production and the amplification factor. However, the regulation of PRO_x as a mitigation target has not been considered before in policy making. A lot of effort has been spent on the emission control of NO_x and VOCs, whereas only few observations of primary radical precursors have been made by far. As the sole change of the ChL which is

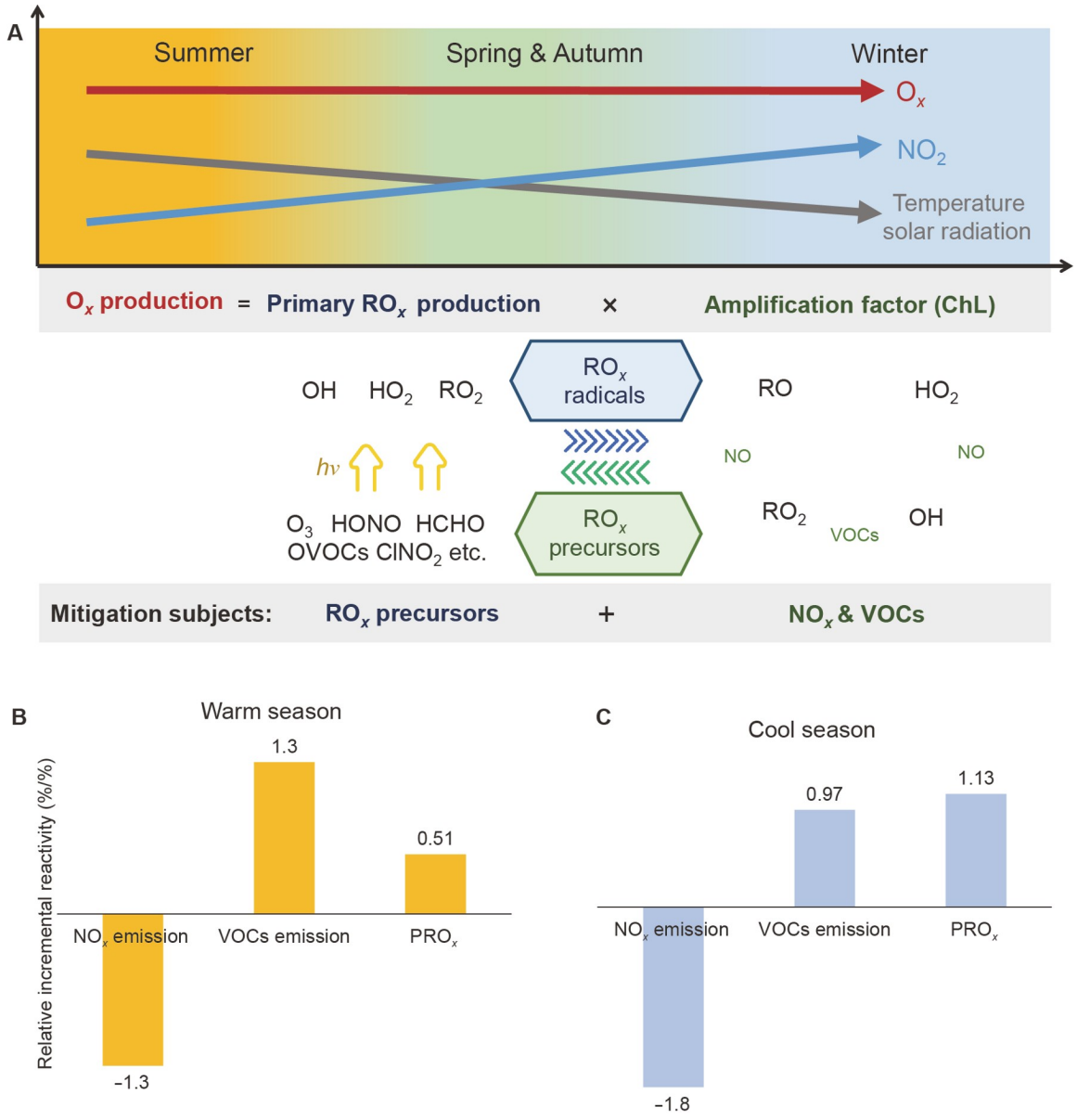

Figure 4 A conceptual diagram for the seasonal variation of the photochemistry and a new O_3 pollution control strategy. (A) From a phenomenon perspective, high and conserved total oxidants were observed from hot to cool seasons in Eastern Chinese conurbations despite a decrease of temperature and solar radiation and increase of NO_2 concentrations. In the framework of the new control strategy, the photochemical O_3 production is split into two components: primary RO_x production and the amplification factor during the OH-HO_2-RO_2 radical cycling (often noted as ChL). In the cool seasons, it is in fact the radical precursors, in addition to the widely regulated species—NO_x and VOCs, that are worth considering as mitigation subjects for the control of primary RO_x production. (B), (C) O_3 relative incremental reactivity of NO_x, VOCs and primary RO_x productions during warm and cool seasons.

mostly modulated by the change of NO_x and VOCs is difficulty for the change of O_x in cool seasons, we hereby propose a new framework, which includes reducing primary production of RO_x as the optimization target, for the control of photochemical pollutions. Sensitivity tests on O_3 productions for both warm and cool seasons (Figures 4B and 4C) show that compared with summer, O_3 is more sensitive to the change of PRO_x during cool seasons, which is even higher than that to the change of VOCs emissions. NO_x control is always

dis-benefit in both seasons (see Methods for details of the plot).

Based on our measurements in Eastern China, direct emissions are a crucial component of the source of radical precursors. Formaldehyde, for example, as the most abundant carbonyl compound in atmosphere, has a primary emission ranged from 10.1% to 50.1% in the YRD region varying with locations and seasons. Relatively high values tend to appear during winter in urban areas and industrial regions, whereas lower values were found in suburban areas during spring and summer (Table S2). On average, the direct emission was reported to contribute 22% to its concentration in the YRD region [29] and up to 52% in Wuhan [30]. Direct HONO emission was found from combustion with a rate of 0.1%±30% ppbv per hour [13] and soil [31–33]. Although the explicit halogen chemistry was not applied in our model due to the lack of ambient measurement of these halogen reservoirs (e.g., $ClNO_2$, Cl_2, BrCl) and the uncertain inventory of primary halogen containing species [34–36], recent studies in China have found significant abundance of chlorine reservoirs, which might act as an important RO_x source and contribute to O_3 pollution [37–40]. Therefore, the control on primary anthropogenic emission of HCl and particulate chlorine ions may also be useful for the control of the primary radical production compared with that of NO_x. Even for the secondary formed radical precursors, the target reduction on the primary RO_x production will help to prioritize the VOCs reduction (i.e., the VOCs with large potentials to generate RO_x radicals). For instance, HCHO, as one of the most important precursors of RO_x, is primarily formed during oxidation of alkenes [41,42]. Ozonolysis of some alkenes can generate great amount of RO_x radicals. Therefore, to reduce the primary radical productions for the cool seasons more studies need to be focused on the emissions of alkenes with fast ozonolysis of high HCHO yield, compared with high alkane or aromatic emissions. Nevertheless, the unrecognized primary radical sources need to be elucidated urgently as it represents roughly half of the total primary radical source which needs to be controlled during cool seasons. This new concept for the O_3 and as well for the secondary particulate matter mitigation strategies in cool seasons may be applicable to other places worldwide.

METHODS

The data

Hourly measurements of O_3, NO_2, CO and $PM_{2.5}$ in Shanghai, YRD, and NCP regions from 2013 to 2019 were obtained from the Ambient Air Quality Monitoring Stations in China (see Figure S1A for the spatial distribution of the observational sites). Fifty-four species of VOCs data in Shanghai were measured by an online high-performance gas chromatograph with a flame ionization detector and mass spectrometer (GC-FID/MS, TH-300-PKU, China) at the campus of the Shanghai Academy of Environmental Sciences (SAES) from 2017 to 2019 with a time resolution of 1 h. Besides, hourly surface meteorological parameters such as temperature, relative humidity and solar radiation during the same period were recorded by the Surface Meteorological Stations in China (see Figure S1C for the spatial distribution). Detailed descriptions of the data are included in Supplementary Information.

Model simulations

The concentrations of OH, HO_2, RO_2, NO, O_3 and other unmeasured secondary species were simulated by a

box model based on the Regional Atmospheric Chemical Mechanism version 2 (RACM2) incorporated with the newly proposed isoprene mechanisms in the base scenario. All primary species including NO, NO_2 and primary VOCs (lumped to model species listed in Table S1) were introduced individually into the model continuously by the time-dependent source function, which was tuned to best match the correspondingly observed values for each bin during the entire modelling period. This approach has been applied previously to simulate high ozone pollution in an oil basin [3]. The concentration of HONO was constrained as 0.02 times the concentration of NO_2 measured [32]. The unmeasured photolysis frequencies were estimated from the parameterization of Master Chemical Mechanism (MCM) and scaled with the ratio of the MCM calculated $j$$NO_2$ and the observed $j$$NO_2$. The details of model constrain parameterization are included in Supplementary Information.

The observation of NO, NO_2, CO, HCHO, C2-C12 VOCs, photolysis constants ($j$$NO_2$, $j$$O^1D$, jHCHO, jHONO and $j$$H_2O_2$) and meteorology parameters (e.g., RH, temperature, planetary boundary layer height) are categorized into nine different bins according to temperature. The model was initialized with the observed NO_x and primary VOCs and O_3 values at 00:00 for each bin in all cases, followed by a 24 h spin-up period to better reproduce the build-up of oxidation products. In order to prevent the unrealistic accumulation of unconstrained species, a first-order loss rate was set to represent mixing and deposition in the model. An up to 3×10^{-5} s^{-1} loss parameter, varying according to boundary layer scale, was applied to the turbulent convective mixing between the mixing layer and aloft. The dry deposition rates for all species were also included in every model simulation, which were negatively related to PBL height. For most species, the deposition rates were all set to 0.02 cm s^{-1} without special consideration. According to reported values in Adon *et al.* [43] and Wesely and Hicks [44], a deposition rate of 0.2 cm s^{-1} was selected for O_3, which was in the reasonable range of values on several kinds of land cover [43,44]. Comparison of model simulation and the observations for the hottest and coolest bins are shown in Figures S12 and S13.

Calculations of the relative incremental reactivity

The applied NO_x and VOCs emission terms were reduced by 10% to estimate the relative incremental sensitivity (RIR) of the calculated daily ozone maximum concentrations which reflected the accumulated ozone production rates per day for the model (see eq. (1)). For the lower temperature condition bins, the test was conducted with the missing PRO_x included since it reproduces the atmospheric chemistry processes better. The RIR for the primary radical sources is estimated by the same way that the primary radical sources were reduced by 10% via the added additional sources, HONO concentration and alkenes emission in the model. It can be easy to identify that the reduction of primary radical sources is mainly contributed by the added additional sources in cool seasons while the reduction for HONO concentrations dominates the overall reduction in warm seasons.

$$\mathrm{RIR} = \Delta O_3\_\mathrm{max} / O_3\_\mathrm{max} / (\Delta X / X),\ X = \text{sources of } NO_x,\ \text{VOCs and } RO_x \text{ radicals.} \quad (1)$$

Data availability

All data and model related codes supporting this research can be accessed with the following link: https://data.mendeley.com/datasets/hjbk3k3j4w/1.

Acknowledgements

We would like to thank Xuefei Ma, Ming Zhou and Yuhan Liu for the insightful discussions on the radical chemistry.

Funding

This work was supported by the Natural Science Foundation of Beijing Municipality (JQ19031), the National Natural Science Foundation of China (21976006, 21522701, and 91544225), the National Research Program for Key Issue in Air Pollution Control (2019YFC0214800 and 2018YFC0213800), and the Science and Technology Commission of the Shanghai Municipality (18QA1403600).

Author contributions

K.L., C.H., and H.W. designed the study. H.W., C.H., and Y.G. collected and analyzed the measurement results in Shanghai, YRD and NCP. S.J. and Q.W. carried out VOCs measurements in Shanghai. K.L., Y. L., W.Q., and X.C. performed the model analysis and interpreted the model results. P. E. and S. L. helped to improve the model simulations. Y.L., K.L., and H.W. wrote the paper. All authors discussed and improved the paper.

Conflict of interest

The authors declare that there are no conflicts of interest to disclose.

Supplementary information

The supporting information is available online at https://doi.org/10.1360/nso/20220013. The supporting materials are published as submitted, without typesetting or editing. The responsibility for scientific accuracy and content remains entirely with the authors.

References

1 Finlayson-Pitts BJ, Pitts JN. Chemistry of the Upper and Lower Atmosphere: Theory, Experiments and Applications. Calif: Academic Press, 2000.

2 Rohrer F, Berresheim H. Strong correlation between levels of tropospheric hydroxyl radicals and solar ultraviolet radiation. *Nature* 2006; **442**: 184–187.

3 Edwards PM, Brown SS, Roberts JM, *et al.* High winter ozone pollution from carbonyl photolysis in an oil and gas basin. *Nature* 2014; **514**: 351–354.

4 Schnell RC, Oltmans SJ, Neely RR, *et al.* Rapid photochemical production of ozone at high concentrations in a rural site during winter. *Nat Geosci* 2009; **2**: 120–122.

5 Lu K, Fuchs H, Hofzumahaus A, *et al.* Fast photochemistry in wintertime haze: Consequences for pollution mitigation strategies. *Environ Sci Technol* 2019; **53**: 10676–10684.

6 Womack CC, McDuffie EE, Edwards PM, *et al.* An odd oxygen framework for wintertime ammonium nitrate aerosol pollution in urban areas: NO_x and VOC control as mitigation strategies. *Geophys Res Lett* 2019; **46**: 4971–4979.

7 Feng T, Zhao S, Zhang X, *et al.* Increasing wintertime ozone levels and secondary aerosol formation in the Guanzhong basin, central China. *Sci Total Environ* 2020; **745**: 140961.

8 Li K, Jacob DJ, Liao H, *et al.* Ozone pollution in the North China Plain spreading into the late-winter haze season. *Proc Natl Acad Sci USA* 2021; **118**: 2015797118.

9 Ren X, Brune WH, Mao J, *et al.* Behavior of OH and HO_2 in the winter atmosphere in New York City. *Atmos Environ* 2006; **40**: 252–263.

10 Kanaya Y, Cao R, Akimoto H, *et al.* Urban photochemistry in central Tokyo: 1. Observed and modeled OH and HO_2 radical concentrations during the winter and summer of 2004. *J Geophys Res* 2007; **112**: D21312.

11 Ma X, Tan Z, Lu K, *et al.* Winter photochemistry in Beijing: Observation and model simulation of OH and HO_2 radicals at an urban site. *Sci Total Environ* 2019; **685**: 85–95.

12 Tan Z, Rohrer F, Lu K, *et al.* Wintertime photochemistry in Beijing: Observations of RO_x radical concentrations in the North China Plain during the BEST-ONE campaign. *Atmos Chem Phys* 2018; **18**: 12391–12411.

13 Rappenglück B, Ackermann L, Alvarez S, *et al.* Strong wintertime ozone events in the Upper Green River basin, Wyoming. *Atmos Chem Phys* 2014; **14**: 4909–4934.

14 Harrison RM, Yin J, Tilling RM, *et al.* Measurement and modelling of air pollution and atmospheric chemistry in the U.K. West Midlands conurbation: Overview of the PUMA Consortium project. *Sci Total Environ* 2006; **360**: 5–25.

15 Heard DE, Carpenter LJ, Creasey DJ, *et al.* High levels of the hydroxyl radical in the winter urban troposphere. *Geophys Res Lett* 2004; **31**: L18112.

16 Wang H, Chen X, Lu K, *et al.* NO_3 and N_2O_5 chemistry at a suburban site during the EXPLORE-YRD campaign in 2018. *Atmos Environ* 2020; **224**: 117180.

17 Liu SC, Trainer M, Fehsenfeld FC, *et al.* Ozone production in the rural troposphere and the implications for regional and global ozone distributions. *J Geophys Res* 1987; **92**: 4191–4207.

18 Zhang YH, Su H, Zhong LJ, *et al.* Regional ozone pollution and observation-based approach for analyzing ozone-precursor relationship during the PRIDE-PRD2004 campaign. *Atmos Environ* 2008; **42**: 6203–6218.

19 Gaudel A, Cooper OR, Ancellet G, *et al*. Tropospheric ozone assessment report: Present-day distribution and trends of tropospheric ozone relevant to climate and global atmospheric chemistry model evaluation. *Elem Sci Anth* 2018; **6**: 39.

20 Murphy J, Day D, Cleary P, *et al*. The weekend effect within and downwind of Sacramento: Part 2. Observational evidence for chemical and dynamical contributions. *Atmos Chem Phys Discuss* 2006; **6**, doi: 10.5194/acpd-6-11971-2006.

21 Ehlers C, Klemp D, Rohrer F, *et al.* Twenty years of ambient observations of nitrogen oxides and specified hydrocarbons in air masses dominated by traffic emissions in Germany. *Faraday Discuss* 2016; **189**: 407–437.

22 Pusede SE, Steiner AL, Cohen RC. Temperature and recent trends in the chemistry of continental surface ozone. *Chem Rev* 2015; **115**: 3898–3918.

23 Tan Z, Lu K, Dong H, *et al.* Explicit diagnosis of the local ozone production rate and the ozone-NO_x-VOC sensitivities. *Sci Bull* 2018; **63**: 1067–1076.

24 Tan Z, Fuchs H, Lu K, *et al.* Radical chemistry at a rural site (Wangdu) in the North China Plain: Observation and model calculations of OH, HO_2 and RO_2 radicals. *Atmos Chem Phys* 2017; **17**: 663–690.

25 Hofzumahaus A, Rohrer F, Lu K, *et al.* Amplified trace gas removal in the troposphere. *Science* 2009; **324**: 1702–1704.

26 Brune WH, Baier BC, Thomas J, *et al.* Ozone production chemistry in the presence of urban plumes. *Faraday Discuss* 2016; **189**: 169–189.

27 Canonaco F, Slowik JG, Baltensperger U, *et al.* Seasonal differences in oxygenated organic aerosol composition: Implications for emissions sources and factor analysis. *Atmos Chem Phys* 2015; **15**: 6993–7002.

28 Kondo Y, Morino Y, Fukuda M, *et al.* Formation and transport of oxidized reactive nitrogen, ozone, and secondary organic aerosol in Tokyo. *J Geophys Res* 2008; **113**: D21310.

29 Su W, Liu C, Hu Q, *et al.* Primary and secondary sources of ambient formaldehyde in the Yangtze River Delta based on ozone mapping and profiler suite (OMPS) observations. *Atmos Chem Phys* 2019; **19**: 6717–6736.

30 Zeng P, Lyu X, Guo H, *et al.* Spatial variation of sources and photochemistry of formaldehyde in Wuhan, Central China. *Atmos Environ* 2019; **214**: 116826.

31 Gall ET, Griffin RJ, Steiner AL, *et al.* Evaluation of nitrous acid sources and sinks in urban outflow. *Atmos Environ* 2016; **127**: 272–282.

32 Liu Y, Lu K, Li X, *et al.* A comprehensive model test of the HONO sources constrained to field measurements at rural North China Plain. *Environ Sci Technol* 2019; **53**: 3517–3525.

33 Oswald R, Behrendt T, Ermel M, *et al.* HONO emissions from soil bacteria as a major source of atmospheric reactive nitrogen. *Science* 2013; **341**: 1233–1235.

34 Fu X, Wang T, Wang S, *et al.* Anthropogenic emissions of hydrogen chloride and fine particulate chloride in China. *Environ Sci Technol* 2018; **52**: 1644–1654.

35 Keene WC, Khalil MAK, Erickson Iii DJ, *et al.* Composite global emissions of reactive chlorine from anthropogenic and natural sources: Reactive chlorine emissions inventory. *J Geophys Res* 1999; **104**: 8429–8440.

36 Liu Y, Fan Q, Chen X, *et al.* Modeling the impact of chlorine emissions from coal combustion and prescribed waste incineration on tropospheric ozone formation in China. *Atmos Chem Phys* 2018; **18**: 2709–2724.

37 Hong Y, Liu Y, Chen X, *et al.* The role of anthropogenic chlorine emission in surface ozone formation during different seasons over eastern China. *Sci Total Environ* 2020; **723**: 137697.

38 Peng X, Wang W, Xia M, *et al.* An unexpected large continental source of reactive bromine and chlorine with significant impact on wintertime air quality. *Natl Sci Rev* 2021; **8**: nwaa304.

39 Tham YJ, Wang Z, Li Q, *et al.* Significant concentrations of nitryl chloride sustained in the morning: investigations of the causes and impacts on ozone production in a polluted region of northern China. *Atmos Chem Phys* 2016; **16**: 14959–14977.

40 Wang T, Tham YJ, Xue L, *et al.* Observations of nitryl chloride and modeling its source and effect on ozone in the planetary boundary layer of southern China. *J Geophys Res Atmos* 2016; **121**: 2476–2489.

41 Li M, Shao M, Li LY, *et al.* Quantifying the ambient formaldehyde sources utilizing tracers. *Chin Chem Lett* 2014; **25**: 1489–1491.

42 Wolfe GM, Kaiser J, Hanisco TF, *et al*. Formaldehyde production from isoprene oxidation across NO_x regimes. *Atmos Chem Phys* 2016; **16**: 2597–2610.

43 Adon M, Galy-Lacaux C, Delon C, *et al*. Dry deposition of nitrogen compounds (NO_2, HNO_3, NH_3), sulfur dioxide and ozone in west and central African ecosystems using the inferential method. *Atmos Chem Phys* 2013; **13**: 11351–11374.

44 Wesely M, Hicks BB. A review of the current status of knowledge on dry deposition. *Atmos Environ* 2000; **34**: 2261–2282.